Journal of Power Sources 245 (2014) 764–771

Contents lists available at SciVerse ScienceDirect

Journal of Power Sources

journal homepage: www.elsevier.com/locate/jpowsour

$Li_4Ti_5O_{12}$ modified with Ag nanoparticles as an advanced anode material in lithium-ion batteries

Michal Krajewski [a], Monika Michalska [b], Bartosz Hamankiewicz [a,d], Dominika Ziolkowska [c], Krzysztof P. Korona [c], Jacek B. Jasinski [e], Maria Kaminska [c], Ludwika Lipinska [b], Andrzej Czerwinski [a,d,*]

[a] Faculty of Chemistry, University of Warsaw, Pasteura 1, 02-093 Warsaw, Poland
[b] Institute of Electronic Materials Technology, Wolczynska 133, 01-919 Warsaw, Poland
[c] Faculty of Physics, University of Warsaw, Hoza 69, 00-681 Warsaw, Poland
[d] Industrial Chemistry Research Institute, Rydygiera 8, 01-793 Warsaw, Poland
[e] Conn Center for Renewable Energy Research, University of Louisville, Louisville, KY 40292, USA

HIGHLIGHTS

- $Li_4Ti_5O_{12}$ of spinel structure was synthesized by a modified solid state method.
- Successful deposition of 2–10 nm silver nanoparticles on $Li_4Ti_5O_{12}$ grains.
- Modification improved $Li_4Ti_5O_{12}$ high-rate performance and cyclability.

ARTICLE INFO

Article history:
Received 13 April 2013
Received in revised form
1 July 2013
Accepted 9 July 2013
Available online 17 July 2013

Keywords:
$Li_4Ti_5O_{12}$
Silver nanoparticles
Li-ion battery
Anode
Solid-state synthesis

ABSTRACT

A three-step solid state synthesis was used to produce powders of spinel phase $Li_4Ti_5O_{12}$ with crystallite size in a few hundred nanometers range. This was followed by surface modification through the deposition of 2–10 nm Ag nanoparticles, as verified by scanning and transmission electron microscopy, X-ray diffraction, X-ray photoelectron spectroscopy, and Raman spectroscopy. The electrochemical performance of these $Li_4Ti_5O_{12}$/*n*-Ag composite powders was examined by chronopotentiometry in three-electrode Swagelok cells. These measurements showed excellent high-rate performance and remarkably good cyclability of the fabricated powders. Specifically, capacity retention in excess of 86% after raising the discharge current from 1C to 10C and less than 6% of capacity loss after 50 charge/discharge cycles at 1C current rate were measured.

1. Introduction

Lithium–titanium oxide with spinel structure – $Li_4Ti_5O_{12}$ (LTO) is one of the promising materials to replace graphitic anodes in lithium-ion batteries. It shows excellent cyclability due to negligible volume change and no structural changes during lithium insertion–extraction ("zero-strain" electrode) [1,2]. Moreover, it has a high operating potential of 1.55 V vs. Li/Li^+, preventing metallic lithium plating during overcharge and hindering the formation of solid-electrolyte interface (SEI) on the surface of the material particles, during LTO cycling between 1 and 3 V [3], which is the main cause of an irreversible lithium loss, raise of the electrode resistance and, in extreme situations, short-circuiting of the cell due to dendrite growth on the negative electrode surface.

The reversible lithium storage mechanism that takes place at the potential range mentioned above, involves the following conversion reaction:

$$Li_4Ti_5O_{12} + 3Li^+ + 3e^- \underset{\text{Oxidation}}{\overset{\text{Reduction}}{\rightleftarrows}} Li_7Ti_5O_{12}. \quad (1)$$

Assuming 100% of the reaction efficiency and including the molar mass of $Li_4Ti_5O_{12}$, yields the theoretical specific capacity of

* Corresponding author. Faculty of Chemistry, University of Warsaw, Pasteura 1, 02-093 Warsaw, Poland.
E-mail addresses: aczerw@chem.uw.edu.pl, andrzej.a.czerwinski@gmail.com (A. Czerwinski).

0378-7753/$ – see front matter © 2013 Elsevier B.V. All rights reserved.
http://dx.doi.org/10.1016/j.jpowsour.2013.07.048

175 mAh g^{-1} for this compound. This and previously mentioned properties make $Li_4Ti_5O_{12}$ a good candidate for various lithium-ion applications, especially when paired with such cathode materials like spinel $LiMn_2O_4$ [4,5] or olivine $LiFePO_4$ [6,7]. However, the low electronic and ionic conductivity, resulting in poor rate capability, remains one of the major factors limiting widespread applications of this material [8]. Huang et al. reported previously, that the surface modification of $Li_4Ti_5O_{12}$ by Ag deposition can greatly improve its high-rate performance [9,10]. Two approaches to create silver deposition on LTO surface have been investigated recently: thermal decomposition of $AgNO_3$ [9] and electroless deposition method [10,11]. Liu et al. [11] have reported higher specific capacity ca. 190 mAh g^{-1} than theoretical one for $Li_4Ti_5O_{12}$/Ag composite with 3.6 wt.% silver concentration but without any explanation of this phenomena.

Here, in this research, we explored an alternative, low temperature approach that enables fabrication of small-sized Ag nanoparticles (n-Ag) on the $Li_4Ti_5O_{12}$ surface. We used this approach to modify the surface of $Li_4Ti_5O_{12}$ powders prepared by a modified solid-state synthesis and observed remarkable improvement of their high-rate capability. In addition, we conducted a systematic and in-depth study on how the rate capability of $Li_4Ti_5O_{12}$ changes with n-Ag content.

2. Experimental

2.1. Synthesis of pristine $Li_4Ti_5O_{12}$ and modification of its surface with Ag nanoparticles

2.1.1. Synthesis of nanocrystalline $Li_4Ti_5O_{12}$

A three-stage solid state synthesis process (Fig. 1) was used to produce nanocrystalline lithium-titanium oxide $Li_4Ti_5O_{12}$ of spinel structure. In the first stage, stoichiometric amounts of lithium carbonate Li_2CO_3 (prepared by Institute of Electronic Materials Technology) and titanium dioxide TiO_2 (99%, Sigma–Aldrich) were used as starting reagents. The powders were mixed together, grinded in an agate mortar and placed in an alumina crucible. The material was heated to 950 °C and annealed for 10 h under air atmosphere. In the second step, the obtained powder was grinded in an agate mortar and heated at 500 °C for 6 h and then at 800 °C for the additional 20 h under air atmosphere. In the third stage, the sample was mixed with ethanol medium and zirconia balls and mechanically grinded for 12 h in a planetary ball mill at a rotation speed of 200 rpm. The mixed reactant was evaporated and subsequently dried at 150 °C for a few hours in air atmosphere. Finally, the powder was grinded in an agate mortar and heated at 500 °C for 6 h and then at 800 °C for additional 20 h under air atmosphere. Long sintering time in the nanocrystalline $Li_4Ti_5O_{12}$ synthesis was conducted to remove the impurities present in prepared powders after each step of mechanical grinding.

2.1.2. Synthesis of $Li_4Ti_5O_{12}$/n-Ag

To synthesize the LTO/n-Ag composites, $AgNO_3$ was dissolved in an ethanol and the prepared nanocrystalline LTO powder was added to obtain a suspension. In order to obtain composites with different n-Ag content, a series of five suspensions were prepared with the Ag to LTO weight ratio of 0.01, 0.02, 0.03, 0.04, and 0.05, respectively. Each mixture was initially stirred for a few hours to obtain a homogenously-dispersed suspension and then air-dried for a few hours at 150 °C. In the last step, the composites were grinded in an agate mortar to obtain fine powder.

2.2. Measurements (SEM, TEM, XPS, Raman spectroscopy, CP)

Phase identification of the prepared samples was carried out by X-ray Diffraction (XRD) using a Siemens D-500 X-ray Powder Diffractometer. XRD patterns were measured between 10 and 60° (2Θ angle) with a Cu K_α radiation source (λ = 1.542 Å). Morphology and particle size of the products were determined by use of a scanning electron microscope (SEM, Cross Beam Auriga, Carl Zeiss) and a transmission electron microscope (TEM, FEI Tecnai F20).

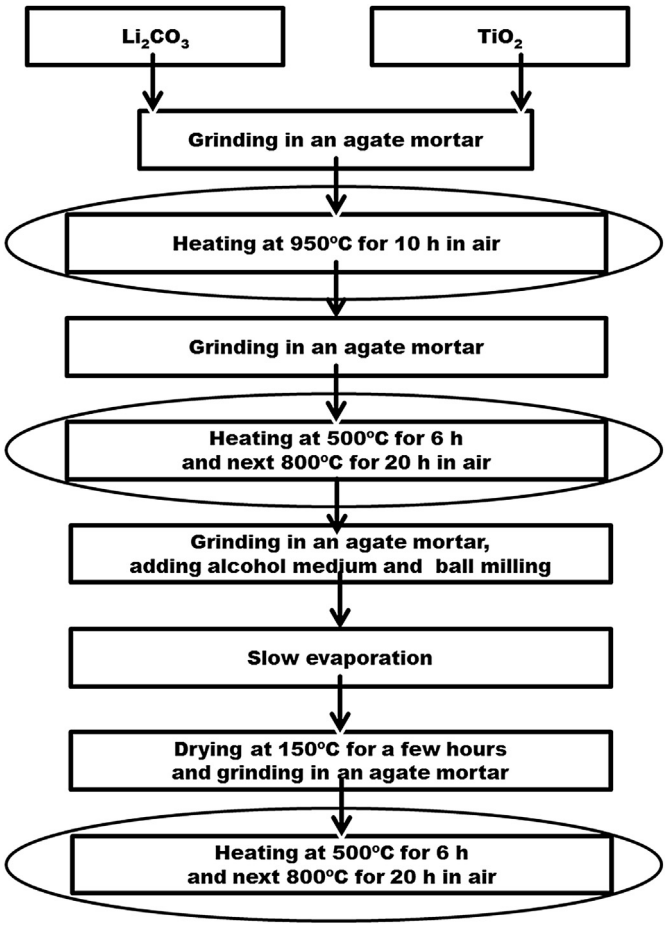

Fig. 1. The flowchart of all stages of solid state synthesis of nanocrystalline $Li_4Ti_5O_{12}$.

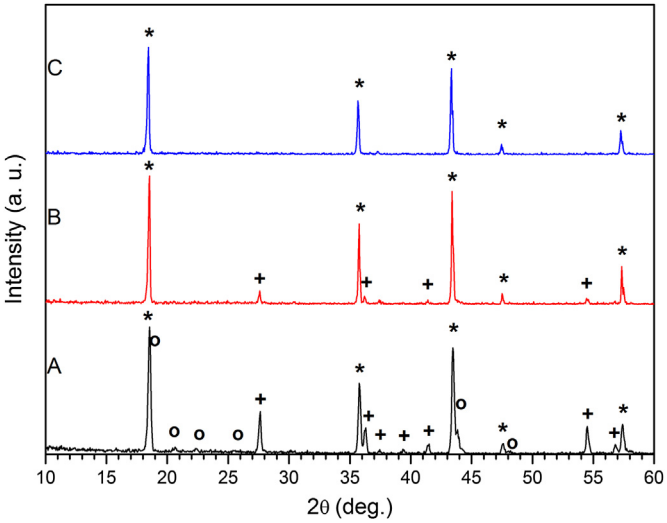

Fig. 2. XRD patterns of samples prepared during synthesis after the first (A), second (B) and third (C) step (* – spinel $Li_4Ti_5O_{12}$, ○ – Li_2TiO_3, + – rutile TiO_2).

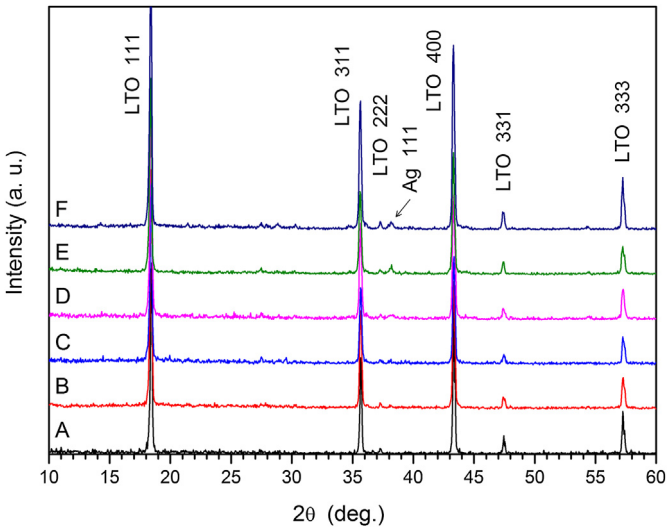

Fig. 3. XRD patterns of pristine (A) and n-Ag modified $Li_4Ti_5O_{12}$: 1% wt. (B), 2% wt. (C), 3% wt. (D), 4% wt. (E) and 5% wt. (F).

High-resolution TEM (HRTEM) mode was also used for the study. The surface analysis was performed using X-ray photoelectron spectroscopy (XPS) and Raman spectroscopy. The Raman spectra were measured using Jobin Yvon T64000 system and Nd:YAG laser (wavelength: 532 nm; maximum power: 2 mW). The XPS measurements were conducted in a VG Scientific MultiLab 3000 ultra-high vacuum surface analysis system equipped with CLAM4 hemispherical electron energy analyzer and a dual-anode (Mg/Al) X-ray source operating at 15 kV of voltage and 10 mA of emission current. Samples were measured using a non-monochromatic Al K_α ($h\nu = 1486.6$ eV) X-ray radiation under the base chamber pressure in the 10^{-9} Torr range. To account for any possible sample charging, a C 1s peak of the intrinsic carbon at 284.5 eV was used for binding energy calibration. The analysis of XPS spectra was performed using XPSPEAK41 software [12]. The fitting was executed using lorenzian–gaussian peak combination and a Shirley baseline subtraction.

For electrochemical measurements, the electrodes were made of $Li_4Ti_5O_{12}$/n-Ag composite grinded with Vulcan XC72R (Cabot) carbon in an agate mortar for 20 min. The obtained powder was added to 5% solution of polyvinylidene fluoride (Alfa Aesar) in *N*-methyl pyrrolidinone (Sigma–Aldrich) and the mixture was homogeneously stirred for 4 h. Such prepared slurry was uniformly coated onto copper foil using Elcometer 3545 and dried in 50 °C for 1 h. Round electrodes were then cut from the foil and pressed in hydraulic press under 200 bar pressure for 1 min followed by vacuum drying at 120 °C for 16 h. The electrode composition was 8:1:1 wt. ratio of $Li_4Ti_5O_{12}$/n-Ag:PVdF:carbon. The cells were assembled in an argon-filled glove-box (MBraun Unilab MB-20-G).

Table 1
Crystallite sizes and lattice parameters for pristine and n-Ag modified $Li_4Ti_5O_{12}$ obtained from XRD measurements.

Compound	Average crystallite size (XRD), nm (±5 nm)	Lattice parameter, Å (±0.001 Å)
A) Pristine	76	8.353
B) 1% n-Ag	56	8.354
C) 2% n-Ag	57	8.353
D) 3% n-Ag	48	8.356
E) 4% n-Ag	55	8.358
F) 5% n-Ag	62	8.358

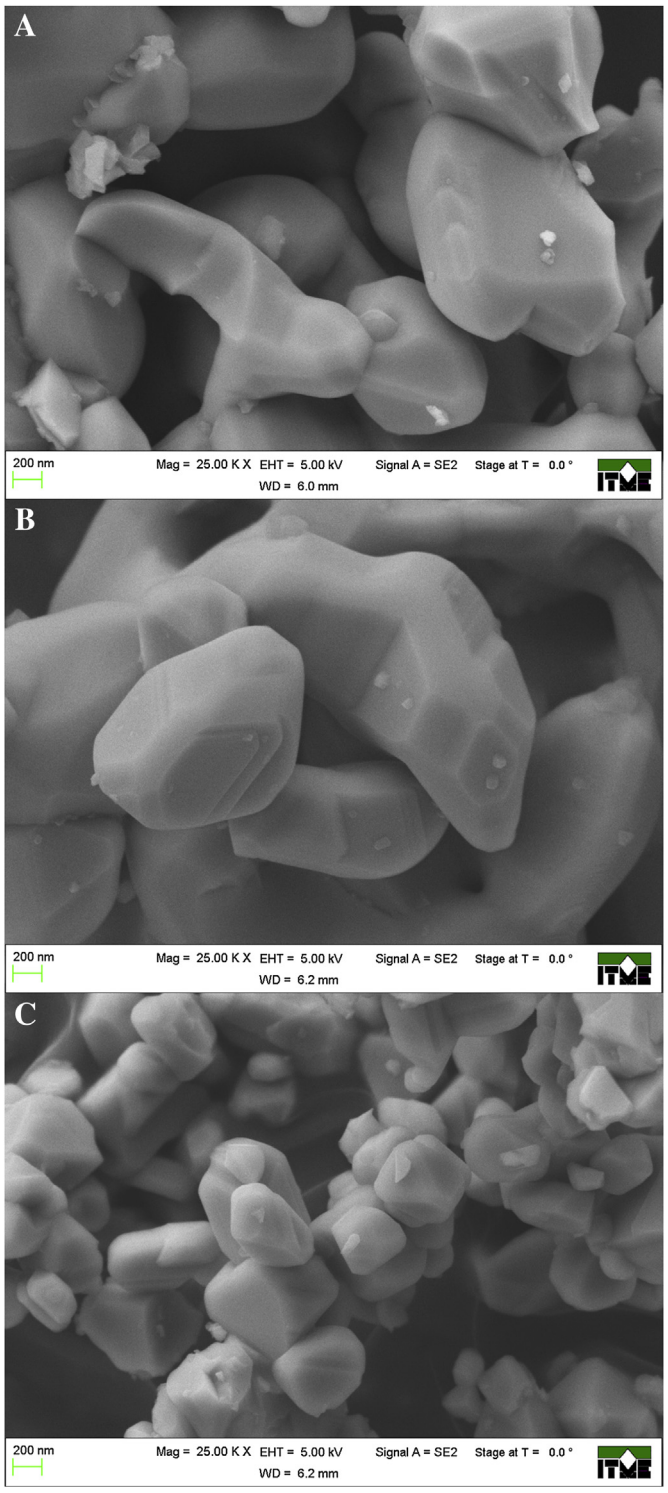

Fig. 4. SEM images of prepared unmodified $Li_4Ti_5O_{12}$ powders after the first (A), second (B) and third (C) step of the synthesis process.

Electrochemical tests were carried out in three-electrode Swagelok systems containing: $Li_4Ti_5O_{12}$/n-Ag working electrode, lithium foil (Sigma–Aldrich) as counter and reference electrodes, 1 M $LiPF_6$ in ethylene carbonate and dimethyl carbonate (1:1) electrolyte (Merck) and Celgard 2400 separator. Experiments were performed using a multichannel battery tester Sollich ATLAS 0961. During cyclability tests, the cells were charged/discharged at 1C (1C

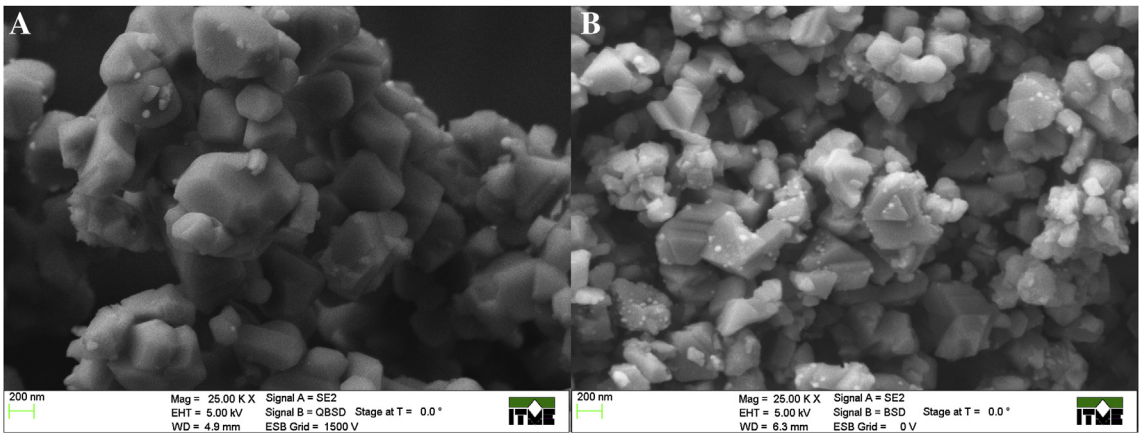

Fig. 5. SEM images of $Li_4Ti_5O_{12}$ powders modified with 1% n-Ag (A) and 5% n-Ag (B).

correspond to current value of 175 mA g^{-1}) current rate while in high-rate tests they were charged using 1C current rate and discharged at various rates. The cells were cycled between 1 and 3 V vs. Li/Li^+.

3. Results and discussion

3.1. XRD results

Fig. 2 shows the XRD patterns of the as-synthesized $Li_4Ti_5O_{12}$ nanopowders after each of the three preparation steps. After the first stage, the samples consisted of 3 phases (pattern A), which were indexed as: (*) spinel $Li_4Ti_5O_{12}$ (49-0207 ICDD), (○) Li_2TiO_3 (33-0831 ICDD) and (+) rutile TiO_2 (21-1276 ICDD). This suggests a relatively poor contact and limited interdiffusion between the grains, hindering the formation of pure-phase LTO powder. During the second step, most of TiO_2 reacted with Li_2TiO_3 and formed $Li_4Ti_5O_{12}$ phase (pattern B), but some TiO_2 impurities were still present. Only the third step consisting of mechanical grinding with alcohol medium and heating removed them completely and produced a single-phase nanocrystalline LTO powder (pattern C). As shown in Fig. 2, all diffraction lines of the powder obtained after the third step could be indexed to the spinel-type phase structure (Fd3m), suggesting, that good contact between the reactant grains, acquired during the ball-milling process, facilitated the efficient solid-state synthesis and lead to successful formation of pure-phase $Li_4Ti_5O_{12}$. Highly-developed specific surface area of the substrates powders, formed during the ball-milling, was certainly responsible for the observed higher reactivity.

One can see, that the synthetic route proposed in this paper might cause some technological issues, due to long sintering time which can lead to high manufacturing cost of pristine $Li_4Ti_5O_{12}$. We simultaneously carried out research about one-step solid state synthesis including only ball milling with subsequent heating in elevated temperature. Preliminary results show, that we acquired pure spinel $Li_4Ti_5O_{12}$ nanopowders. However, this is not the subject of this paper and it will not be discussed here.

Fig. 3 shows the XRD patterns of the pure and n-Ag-modified $Li_4Ti_5O_{12}$ powders. For each sample, including those with high concentration of Ag, all the peaks associated with LTO are in good agreement with the spinel phase $Li_4Ti_5O_{12}$ pattern confirming that modifying the surface of pristine $Li_4Ti_5O_{12}$ does not lead to any phase segregation. The additional peak at around 38°, observed in the modified sample, showed its intensity scaling up with the increase of Ag content and was identified as the (111) reflection of metallic Ag phase (04-0783 ICDD). A systematic appearance of this peak indicated that metallic Ag nanoparticles were successfully deposited on the surface of $Li_4Ti_5O_{12}$. However, the mechanism of

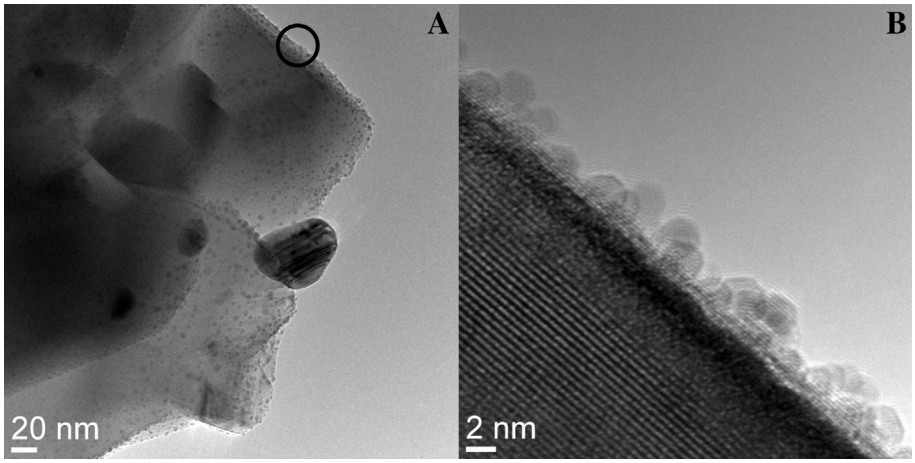

Fig. 6. TEM images of $Li_4Ti_5O_{12}$ powders modified with 5% n-Ag. A low-magnification image showing several grains (A) and HRTEM image of the surface area of one of the $Li_4Ti_5O_{12}$ crystallites (B). A single-crystalline nature of the $Li_4Ti_5O_{12}$ grain is clearly visible in this HRTEM image. In addition, 2 nm-large Ag nanoparticles, deposited on the surface, are also visible.

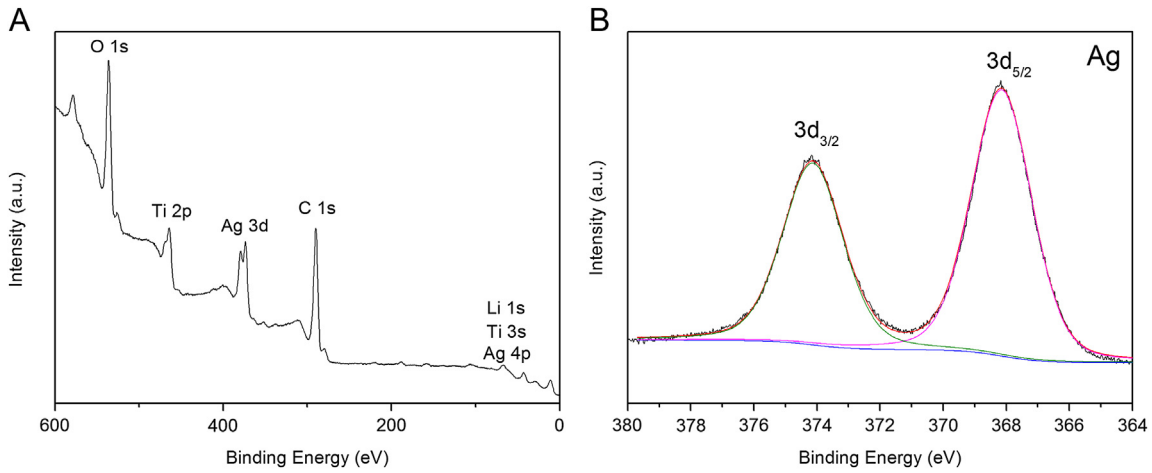

Fig. 7. XPS spectra of $Li_4Ti_5O_{12}$ modified with 5% n-Ag. Low-resolution survey spectrum (A) and high-resolution spectrum of the 380–364 eV range (B).

n-Ag particles precipitation is not fully understood, yet. Since no reducing agent was used to form LTO/n-Ag composites and the powders were not annealed at high temperature needed for complete thermal decomposition of silver nitrate, we suggest, that the preparation product was directly involved in the silver ions reduction. Also, there is a possibility, that the process of silver cations reduction occurred simultaneously with silver nitrate photolysis [13] and/or the partial thermal decomposition of silver nitrate. However, further studies are needed for complete understanding of the precipitation mechanism.

Lattice parameters of the $Li_4Ti_5O_{12}$ powders and their average crystallite sizes, calculated based on the XRD patterns shown in Fig. 3, are listed in Table 1. No significant change with the Ag content was observed. In particular, for all samples, the average crystallites sizes of LTO (estimated from the Scherrer equation) were in the range of 50–60 nm. No crystallite size of Ag nanoparticles was estimated from the XRD data due to very low peak intensities.

3.2. SEM and TEM analysis

Surface morphologies of $Li_4Ti_5O_{12}$ powders after each preparation step are shown in SEM images presented in Fig. 4. After the first, as well as, the second step, the powders consist of large crystallites with well-developed surface faceting (Fig. 4A and B). Clear surface faceting and well-developed crystallites are also observed after the third step of the preparation process (Fig. 4C). However, in this case the crystallite sizes are much smaller (~200–500 nm compared to ~2–3 μm), as expected after the ball-milling process. Thus, the SEM study, similarly to XRD, indicates that the ball-milling process has a very high impact on $Li_4Ti_5O_{12}$ synthesis. The SEM images from powders with different n-Ag content (Fig. 5) indicate that the morphology of $Li_4Ti_5O_{12}$ does not change during n-Ag deposition. Similarly to the pure sample, the Ag-modified powders consisted of well-developed crystallites with cubic-like morphology, faceted walls, and sizes in the range of 200–500 nm. The only significant difference in this case was an additional presence of many small (ca. 10 nm) Ag nanoparticles densely dispersed on the surface of $Li_4Ti_5O_{12}$ crystallites. As indicated by SEM images, the concentration of these Ag nanoparticles was increasing with the increase of concentration of $AgNO_3$ used in synthesis.

SEM findings were consistent with TEM examination. Additionally, HRTEM study confirmed single-crystalline nature of $Li_4Ti_5O_{12}$ particles. Similarly to SEM observations, TEM images

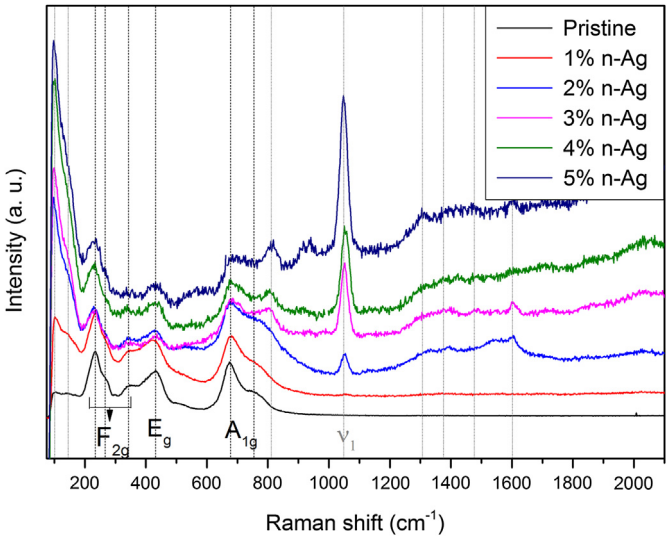

Fig. 8. Raman spectra of pristine and n-Ag modified $Li_4Ti_5O_{12}$.

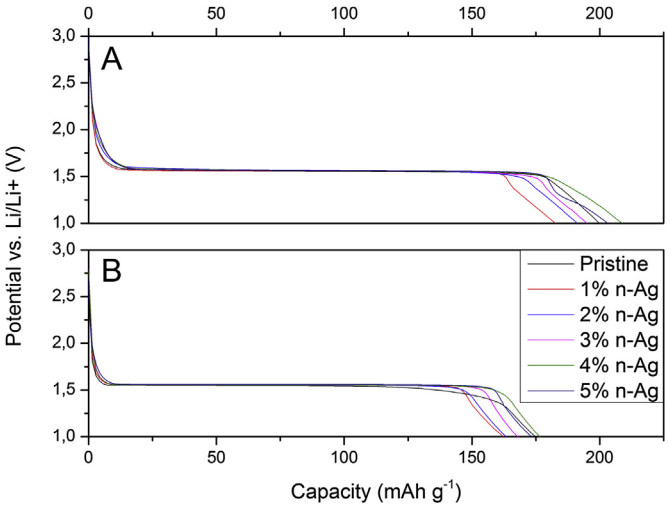

Fig. 9. 1st (A) and 2nd (B) discharge profiles of pristine and n-Ag modified $Li_4Ti_5O_{12}$ at 1C current rate.

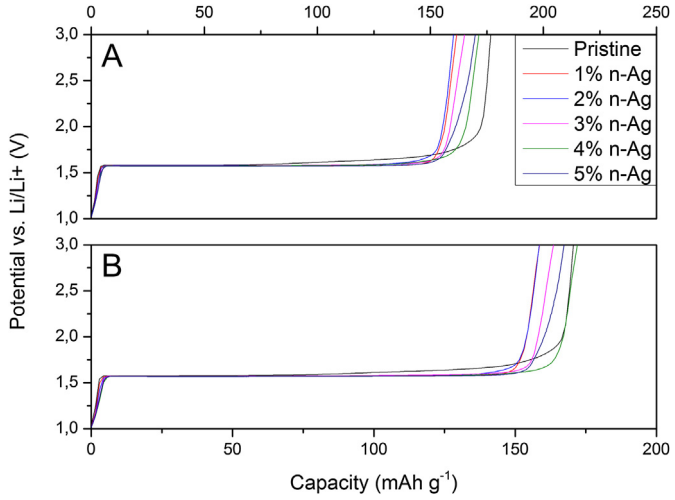

Fig. 10. 1st (A) and 2nd (B) charge profiles of pristine and n-Ag modified $Li_4Ti_5O_{12}$ at 1C current rate.

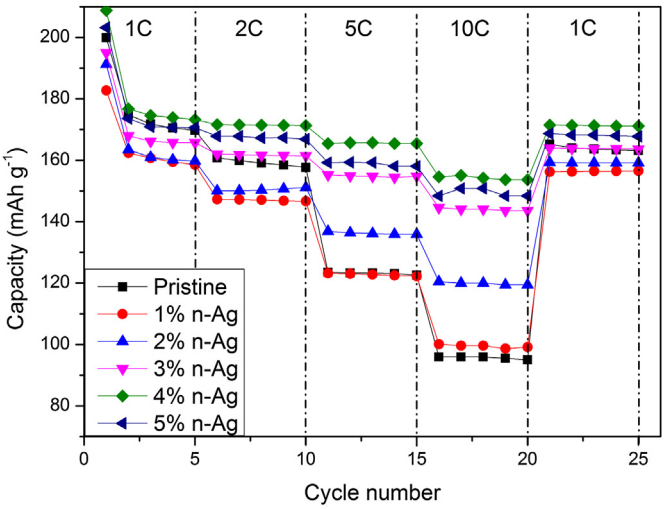

Fig. 11. Rate capability of pristine and n-Ag modified $Li_4Ti_5O_{12}$.

showed ca. 10 nm-sized Ag nanoparticles on the surface of $Li_4Ti_5O_{12}$ crystallites. Furthermore, HRTEM images showed also that the surface of $Li_4Ti_5O_{12}$ crystallites was densely covered by much smaller (ca. 2 nm) Ag nanoparticles (Fig. 6). The measurements indicated that the coverage was directly related to the Ag content, i.e. higher concentration of $AgNO_3$ used during the synthesis, resulted in higher density of Ag nanoparticles on surface of the $Li_4Ti_5O_{12}$ crystallites.

3.3. XPS

The surface chemistry of the fabricated $Li_4Ti_5O_{12}$ powders was studied using XPS analysis and high-resolution spectra of elemental lines were carefully analyzed to achieve valency and bonding information. For instance, the analysis of the measured asymmetric O 1s peak yielded two dominant components, one at 530.3 eV and the other at 532.5 eV, which corresponded to Ti–O bonding in a spinel $Li_4Ti_5O_{12}$ structure and chemisorbed oxygen at the surface of spinel crystallites, respectively [14–16]. For titanium, the measured Ti 2p doublet peak with $2p_{3/2}$ line at 458.7 and $2p_{1/2}$ line at 464.2 eV was assigned to titanium in the IV oxidation state [15–18]. Similar analysis in the Ag 3d region showed a single doublet line with components at 368.1 and 374.1 eV (see Fig. 7), which were identified as the Ag $3d_{5/2}$ and Ag $3d_{3/2}$ lines of metallic silver [11], confirming that Ag nanoparticles deposited on the surface of $Li_4Ti_5O_{12}$ powders were in the pure metallic state. The high-resolution spectra of low binding energy region showed a weak Li 1s peak at 55 eV originated from the Li–O bond, Ti 3p peak with $3p_{1/2}$ line at 36.8 eV, and a peak at 61.6 eV consisting of Ti 3s and Ag $4p_{3/2}$ components [15].

3.4. Raman spectroscopy

Interesting results were obtained from Raman spectroscopy. As expected, the measurements of the unmodified $Li_4Ti_5O_{12}$ powder showed typical $Li_{4/3}Me_{5/3}O_4$ spinel spectra with all five active Raman phonon modes ($A_{1g} + E_g + 3F_{2g}$) as predicted for cubic spinel $Li_4Ti_5O_{12}$ [19–21]. For instance, a strong band at 678 cm^{-1} (A_{1g}) with the shoulder at 754 cm^{-1}, assigned to the stretching vibrational mode of Ti–O covalent bonding in TiO_6 octahedra [19,20,22], was observed. Also, the stretching vibrational mode of Li–O ionic bonds located in LiO_4 tetrahedra (E_g) was present at 431 cm^{-1} [19,20,22]. Finally, lithium, octahedrally-coordinated by oxygen, produced three bands (F_{2g}) at 342 cm^{-1}, 266 cm^{-1} and 233 cm^{-1} [22]. The lines had width (FWHM) of about 50 cm^{-1} what confirmed good crystal quality of the samples.

The spectra of Ag-modified samples (Fig. 8) showed additional sharp (FWHM = 30 cm^{-1}) peaks, which could be assigned to the $AgNO_3$ structure. The strongest peak at 1049 cm^{-1} corresponded to the symmetric stretching vibration of NO_3 (ν_1) [23,24]. Second peak, the asymmetric stretching vibrational mode of NO_3 (ν_3) appeared in the spectra above 1300 cm^{-1} [23,24]. Moreover, strong peaks at 105 cm^{-1} with the shoulder at 145 cm^{-1}, originating from the lattice modes (vibrational and translational) of $AgNO_3$, were also observed [23,24]. The other nitrate vibrational modes of NO_3 such as out-of-plane bending and in-plane bending were very weak and hardly visible in the spectra [23,24]. The comparison of Raman spectra of the Ag-modified materials showed, that $AgNO_3$ coating suppressed the intensities of $Li_4Ti_5O_{12}$ peaks. Therefore, for the ease of comparison, all spectra present in Fig. 8 were normalized to the A_{1g} line of $Li_4Ti_5O_{12}$. This helps to notice that the intensity of $AgNO_3$ peaks was increasing with the increase of silver nitrate amount used during the modification process. It is known that Ag particles

Table 2
Results of high-rate CP tests.

Compound	Electrode loading [mg cm^{-2}]	1C 1st dis. cap. [mAh g^{-1}]	1C 2nd dis. cap. [mAh g^{-1}]	2C dis. cap. [mAh g^{-1}]	5C dis. cap. [mAh g^{-1}]	10C dis. cap. [mAh g^{-1}]	Capacity retained at 10C [%] (±0.01%)
Pristine	2.02 ± 0.16	199.90 ± 19.41	174.85 ± 16.98	160.87 ± 15.62	123.59 ± 12.00	95.97 ± 9.32	54.89
1% n-Ag	1.90 ± 0.16	182.71 ± 19.03	162.40 ± 16.92	147.29 ± 15.34	123.23 ± 12.84	100.13 ± 10.43	61.65
2% n-Ag	2.06 ± 0.02	191.26 ± 1.86	163.50 ± 1.59	150.10 ± 1.46	136.89 ± 1.33	120.49 ± 1.17	73.69
3% n-Ag	2.10 ± 0.16	195.05 ± 18.94	167.96 ± 16.31	162.04 ± 15.73	155.24 ± 15.07	144.56 ± 14.04	86.07
4% n-Ag	2.45 ± 0.16	208.82 ± 17.55	176.72 ± 14.85	171.60 ± 14.42	165.46 ± 13.90	154.62 ± 12.99	87.49
5% n-Ag	1.93 ± 0.16	203.26 ± 16.35	173.56 ± 13.96	167.85 ± 13.50	159.23 ± 12.81	148.40 ± 11.94	85.51

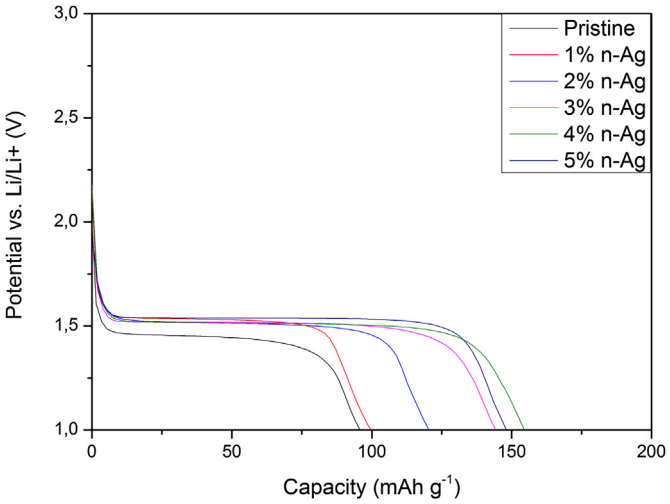

Fig. 12. Discharge curves of pristine and n-Ag modified $Li_4Ti_5O_{12}$ at 10C current rate.

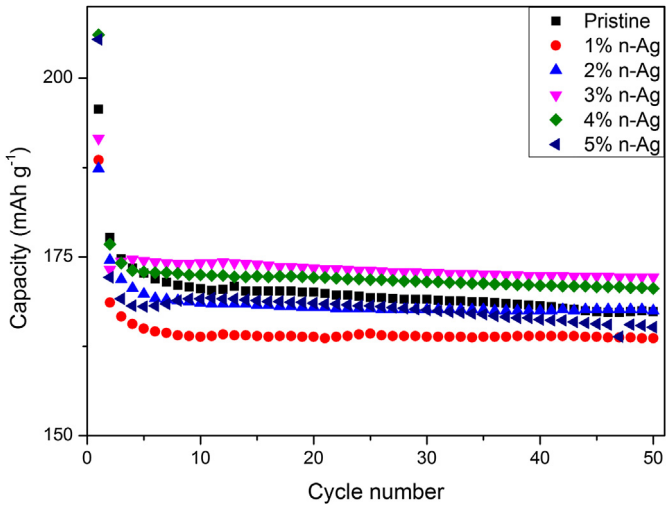

Fig. 13. Cyclability of pristine and n-Ag modified $Li_4Ti_5O_{12}$.

can induce surface enhanced Raman scattering effect [25]. It is possible that the insensible residue of $AgNO_3$ (unnoticed by other techniques) was adsorbed on the metallic Ag spheres and exhibited enhanced Raman signals. Depending on the origin of this enhancement ("electromagnetic" or "chemical"), the increase of vibrational modes intensities can appear even by a factor of $\sim 10^6$ [25]. The appearance of the $AgNO_3$ lines indicated, that its decomposition to the metallic silver was not fully complete and the silver nitrate still partially covered the surface of Ag precipitates and $Li_4Ti_5O_{12}$ crystals.

3.5. Electrochemistry

3.5.1. High-rate tests

Figs. 9 and 10 show the first and the second discharge and charge curves of pristine and modified $Li_4Ti_5O_{12}$ powders at 1C rate. The process of lithium intercalation/deintercalation into/out of the $Li_4Ti_5O_{12}$ framework occurred at a stable potential plateau of 1.55 V vs. Li/Li^+ for every examined sample. The discharge capacities obtained from the cells operating at 1C current rate are listed in Table 2. For each sample, specific capacity delivered from the cells at first discharge was higher than the theoretical value of 175 mAh g^{-1} for lithium–titanium oxide. The extra charge originated from some non-intercalation processes, related to electrode forming, as it was not observed in the second discharge. This behavior could be related to the corrosion of the copper current collector and formation of a SEI layer. The difference between the first and the second discharge curve, occurring between 2.2 and 1.6 V, originated from the reduction of copper oxides to metallic Cu and precipitation of Li_2O [26,27]. However, more studies of these phenomena are needed to better understand this process.

As evident from Fig. 9, the modification of the surface with Ag nanoparticles had no effect on capacity of $Li_4Ti_5O_{12}$ during discharge at 1C rate. However, after raising the current, the examined samples behavior began to differ, which is depicted in Fig. 11. At 10C rate (Fig. 12), each addition of n-Ag resulted in higher specific discharge capacity, with maximum of 154.62 ± 12.99 mAh g^{-1} for 4 wt.% of n-Ag and higher working potential compared to unmodified lithium–titanium oxide. As there was conductive carbon present in both pure and modified electrodes, the higher capacity for $Li_4Ti_5O_{12}$/n-Ag composites can be attributed only to metallic silver deposition. One can see, that after reaching 3 wt.% of n-Ag, the specific capacities at 10C rate did not change significantly. Worth noticing is the fact, that each sample with n-Ag addition greater than 3 wt.% retained ~86% of its specific capacity, ~30% more than unmodified $Li_4Ti_5O_{12}$, while raising the discharge current from 1C to 10C, which is better than previously reported [9–11]. It seems therefore, that modifying the surface of $Li_4Ti_5O_{12}$ with uniformly deposited Ag nanoparticles resulted in faster electron transport between material grains and better contact with current collector, thus leading to improved high-rate capabilities of modified samples.

3.5.2. Cyclability tests

Fig. 13, as well as, Table 3 present the results of cyclability tests performed on pristine and n-Ag modified lithium–titanium oxide. The electrodes examined in these experiments also showed higher than theoretical specific capacity at first discharge, suggesting other electrochemical processes involved at the first cycle. After 50 cycles, samples retained more than 94% of the second discharge specific capacity (with maximum of 99.40 ± 0.01% for 3 wt.% n-Ag added). Each addition of silver nanoparticles reduced the capacity loss and for each n-Ag composite the loss was less than 4%. Therefore, it seems that uniformly distributed n-Ag particles on surface of $Li_4Ti_5O_{12}$ prevented electrode degradation during cycling and kept LTO grains in contact with the current collector.

Table 3
Results of cyclability CP tests.

Compound	Electrode loading [mg cm^{-2}] (±0.16 mg cm^{-2})	1st dis. cap. [mAh g^{-1}]	2nd dis. cap. [mAh g^{-1}]	50th dis. cap. [mAh g^{-1}]	Capacity retained after 50th cycle [%] (±0.01%)
Pristine	1.70	195.63 ± 22.49	177.70 ± 20.43	167.36 ± 19.24	94.18
1% n-Ag	1.90	188.54 ± 19.64	168.65 ± 17.57	163.65 ± 17.05	97.04
2% n-Ag	1.28	187.34 ± 29.27	174.53 ± 27.27	167.50 ± 26.17	95.97
3% n-Ag	1.94	191.56 ± 19.95	173.23 ± 18.04	172.19 ± 17.94	99.40
4% n-Ag	2.03	206.06 ± 20.81	176.77 ± 17.86	170.61 ± 17.23	96.51
5% n-Ag	1.71	205.42 ± 24.75	172.17 ± 20.74	165.18 ± 19.90	95.94

4. Conclusions

We successfully synthesized pristine lithium–titanium oxide using modified solid-state method. The three-step synthesis was required to obtain a powder without any phase impurities. We also successfully modified the prepared $Li_4Ti_5O_{12}$ with uniformly dispersed Ag nanoparticles. XRD, Raman spectroscopy and XPS measurements clearly showed that Ag in metallic form was deposited on the surface of lithium–titanium oxide particles. Raman spectroscopy also indicated the presence of $AgNO_3$ suggesting, that the deposition reaction was not fully efficient. From TEM measurements we estimated the size of n-Ag particles to be between 2 and 10 nm.

Electrochemical behavior of obtained powders was examined by chronopotentiometry. At the first discharge, every sample delivered charge greater than the one expected from theoretical calculations. This behavior was attributed to electrode activation processes or formation of a SEI layer on the copper current collector. The electrochemical testing showed that the high-rate performance of $Li_4Ti_5O_{12}$ was greatly enhanced by modifying the surface with Ag nanoparticles. The samples with more than 3 wt.% of n-Ag retained ~86% of their capacity while raising the current from 1C to 10C. The cyclability of examined powders was also at the high level. The electrodes retained more than 94% of their specific capacity after 50 cycles of charge/discharge processes, while using 1C current rate. Moreover, every modification of Ag nanoparticles reduced the capacity loss by a 2–5%. All these properties could be related to uniform distribution of silver nanoparticles on the surface of $Li_4Ti_5O_{12}$ grains, which resulted in faster electron transport between the LTO particles, better contact with current collector and slower electrode degradation. Also, taking into account both high-rate and cyclability tests, we estimated an optimal silver nanoparticles amount to be 3 wt.%.

There is a common agreement, that surface modification of electrode materials with highly conductive particles or films is a very successful approach to enhance their electrochemical performance. Our work reported in this paper demonstrated, that highly-dispersed Ag nanoparticles on the surface of $Li_4Ti_5O_{12}$ grains greatly improve high-rate capability and cyclability of such materials. Our composite can be used as an example, how homogenously dispersed conductive particles improve electrochemical properties of the materials needed for next generation of Li-ion batteries. We are expecting similar results with other, selected metals.

Acknowledgments

This work was supported by The National Science Centre (NCN) through the research grant DEC-2011/03/N/ST5/04389. M. Michalska would like to thank for the scholarship awarded by the Mazovia Voivodeship Office. The work of D. Ziolkowska was supported by the Foundation for Polish Science International PhD Projects Programme co-financed by the EU European Regional Development Fund. The work of J.B. Jasinski was supported by the US Department of Energy EPSCoR Program.

References

[1] S. Panero, P. Reale, F. Ronci, B. Scrosati, P. Perfetti, V.R. Ablertini, Phys. Chem. Chem. Phys. 3 (2001) 845–847.
[2] T. Ahzuku, A. Ueda, N. Yamamoto, J. Electrochem. Soc. 142 (1995) 1431–1435.
[3] J. Shu, J. Solid State Electrochem. 13 (2009) 1535–1539.
[4] I. Belharouak, Y.-K. Sun, W. Lu, K. Amine, J. Electrochem. Soc. 154 (2007) A1083–A1087.
[5] A. Du Pasquier, C.C. Huang, T. Spitler, J. Power Sources 186 (2009) 508–514.
[6] K. Zaghib, M. Dontigny, A. Guerfi, P. Charest, I. Rodrigues, A. Mauger, C.M. Julien, J. Power Sources 196 (2011) 3949–3954.
[7] K. Zaghib, M. Dontigny, A. Guerfi, J. Trottier, J. Hamel-Paquet, V. Gariepy, K. Galoutov, P. Hovington, A. Mauger, H. Groult, C.M. Julien, J. Power Sources 216 (2012) 192–200.
[8] C.Y. Ouyang, Z.Y. Zhong, M.S. Lei, Electrochem. Commun. 9 (2007) 1107–1112.
[9] S. Huang, Z. Wen, J. Zhang, Z. Gu, X. Xu, Solid State Ionics 177 (2006) 851–855.
[10] S. Huang, Z. Wen, J. Zhang, X. Yang, Electrochim. Acta 52 (2007) 3704–3708.
[11] Z. Liu, N. Zhang, Z. Wang, K. Sun, J. Power Sources 205 (2012) 479–482.
[12] R. Kwok, Department of Chemistry, Chinese University of Hong Kong, XPSPEAK Version 4.1 software.
[13] Y.-H. Lin, K.-T. Chen, J.-R. Ho, Jpn. J. Appl. Phys. 50 (2011) 065002.
[14] Y. Shi, L. Wen, F. Li, H.-M. Cheng, J. Power Sources 196 (2011) 8610–8617.
[15] M. Adler, B. Laughlin, S.G. Lieb, Phys. Chem. Chem. Phys. 1 (1999) 5327–5331.
[16] C.-T. Hsieh, I.-L. Chen, Y.-R. Jiang, J.-Y. Lin, Solid State Ionics 201 (2011) 60–67.
[17] Y. Zhao, G. Liu, L. Liu, Z. Jiang, J. Solid State Electrochem. 13 (2009) 705–711.
[18] A. Sivashanmugam, S. Gopukumar, R. Thirunakaran, C. Nithya, S. Prema, Mater. Res. Bull. 46 (2011) 492–500.
[19] L. Aldon, P. Kubiak, M. Womes, J.C. Jumas, J. Olivier-Fourcade, J.L. Tirado, J.I. Corredor, C. Perez Vicente, Chem. Mater. 16 (2004) 5721–5725.
[20] C.M. Julien, K. Zaghib, Electrochim. Acta 50 (2004) 411–416.
[21] D.G. Kellerman, V.S. Gorshkov, E.V. Shalaeva, B.A. Tsaryev, E.G. Vovkotrub, Solid State Sci. 14 (2012) 72–79.
[22] T. Nakazawa, V. Grismanos, D. Yamaki, Y. Katano, T. Aruga, Nucl. Instrum. Methods Phys. Res. B 206 (2003) 166–170.
[23] I. Martina, R. Wiesinger, D. Jembrih-Simburger, M. Schreiner, e-Preserv. Sci. 9 (2012) 1–8.
[24] K. Balasubrahmanyam, G.J. Janz, J. Chem. Phys. 57 (1972) 4084–4088.
[25] Iven Pockrand, Springer Tracts in Mod. Phys. 104 (1984).
[26] J. Shu, M. Shui, F. Huang, D. Xu, Y. Ren, L. Hou, J. Cui, J. Xu, Electrochim. Acta 56 (2011) 3006–3014.
[27] S.-T. Myung, Y. Hitoshi, Y.-K. Sun, J. Mater. Chem. 21 (2011) 9891–9911.